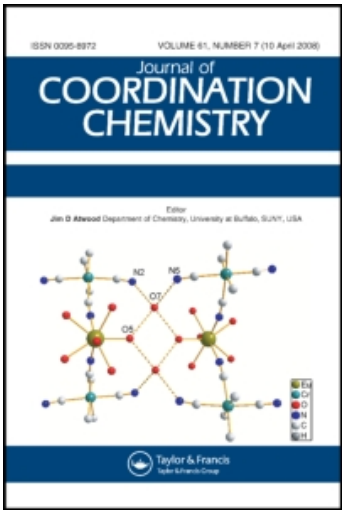

Journal of Coordination Chemistry
Publication details, including instructions for authors and subscription information:
http://www.informaworld.com/smpp/title~content=t713455674

Synthesis, crystal structure, antibacterial activities, and DNA-binding studies of a new μ-oxamido-bridged binuclear copper(II) complex

Yan-Tuan Li[a]; Chun-Yuan Zhu[a]; Zhi-Yong Wu[b]; Man Jiang[b]; Cui-Wei Yan[c]
[a] Marine Drug & Food Institute, Ocean University of China, Qingdao, P.R. China [b] Key Laboratory of Marine Drug, Chinese Ministry of Education, Qingdao, P.R. China [c] College of Marine Life Science, Ocean University of China, Qingdao, P.R. China

To cite this Article Li, Yan-Tuan , Zhu, Chun-Yuan , Wu, Zhi-Yong , Jiang, Man and Yan, Cui-Wei(2009) 'Synthesis, crystal structure, antibacterial activities, and DNA-binding studies of a new μ-oxamido-bridged binuclear copper(II) complex', Journal of Coordination Chemistry, 62: 23, 3795 — 3809
To link to this Article: DOI: 10.1080/00958970903171078
URL: http://dx.doi.org/10.1080/00958970903171078

Journal of Coordination Chemistry
Vol. 62, No. 23, 10 December 2009, 3795–3809

Synthesis, crystal structure, antibacterial activities, and DNA-binding studies of a new μ-oxamido-bridged binuclear copper(II) complex

YAN-TUAN LI*†, CHUN-YUAN ZHU†, ZHI-YONG WU‡, MAN JIANG‡ and CUI-WEI YAN*§

†Marine Drug & Food Institute, Ocean University of China, 5 Yushan Road, Qingdao, 266003, P.R. China
‡Key Laboratory of Marine Drug, Chinese Ministry of Education, Ocean University of China, Qingdao, P.R. China
§College of Marine Life Science, Ocean University of China, Qingdao, 266003, P.R. China

(*Received 3 March 2009; in final form 19 May 2009*)

A new μ-oxamido-bridged dicopper(II) complex, $Cu_2(heap)(NO_3)_2$ (**1**), where heap is the dianion of N,N′-bis(N-hydroxyethylaminopropyl)oxamide, has been synthesized and characterized by elemental analysis, molar conductivity, IR and electronic spectral studies, and X-ray single-crystal diffraction. The complex consists of a neutral centro-symmetric binuclear copper(II) unit with an inversion center at the midpoint of the $Cl-Cl^i$ bond. The copper(II) has square-pyramidal coordination geometry and the bridging heap adopts a *bis*-tetradentate conformation. The binuclear units are linked into a 3-D framework by $N-H\cdots O$, $O-H\cdots O$, and $C-H\cdots O$ hydrogen bonds. Due to weak coordination between copper(II) and nitrate, the neutral dicopper(II) units are present as binuclear cations and nitrate anions in solution. Antibacterial assays indicate that the complex shows better activity than the ligand. Interactions of the complex with herring sperm DNA (*HS*-DNA) have been investigated by using cyclic voltammetry, UV absorption titrations, ethidium bromide fluorescence displacement experiments, and viscometry measurements. The results suggest that the binuclear copper(II) complex interacts with *HS*-DNA by electrostatic interaction with intrinsic binding constant of $3.33 \times 10^4\,M^{-1}$.

Keywords: Crystal structure; Binuclear copper(II) complex; μ-Oxamido-bridge; Antibacterial activities; DNA interactions

1. Introduction

Coordination chemistry of dicopper(II) complexes has become a fascinating area owing to the discovery of the active site in several copper-containing enzymes such as tyrosinase and the development of functional materials showing interesting magnetic properties [1, 2]. Interactions of dicopper(II) complexes with DNA have also attracted considerable attention [3–5] for possible applications in the design of new and more efficient drugs targeted to DNA.

*Corresponding authors. Email: yantuanli@ouc.edu.cn; cuiweiyan@ouc.edu.cn

ISSN 0095-8972 print/ISSN 1029-0389 online
DOI: 10.1080/00958970903171078

It is well known that N,N′-bis(substituent)oxamides are good candidates in forming polynuclear complexes because their coordinating ability toward transition-metal ions can be tuned by changing the nature of the amide substituents [6–10]; this family of ligands has played an important role in coordination chemistry [6, 8]. Much effort has been devoted to the magnetic studies of dinuclear copper(II) complexes bridged by oxamido [9, 10]. However, DNA-binding properties of dicopper(II) complexes with oxamido-bridges have received limited attention. Therefore, we synthesized dicopper(II) complexes with oxamido-bridge to gain insight into the DNA-binding properties as part of our continuous work on the syntheses and properties of the complexes bridged by oxamido groups [11–15]. In this article, we report the synthesis, crystal structure, antibacterial activities, and DNA-binding properties of a new dicopper(II) complex bridged by N,N′-bis(N-hydroxyethylaminopropyl)oxamido (heap), $Cu_2(heap)(NO_3)_2$ (**1**).

2. Experimental

2.1. *Materials*

All reagents used were of analytical grade. The ligand N,N′-bis(N-hydroxyethylaminopropyl)oxamide (H_2heap) was synthesized according to the reported method [6]. Herring sperm DNA (*HS*-DNA) was obtained from Sigma Corp. and used as received.

2.2. *Synthesis of $Cu_2(heap)(NO_3)_2$ (1)*

A solution of copper(II) nitrate trihydrate (120.8 mg, 0.5 mmol) dissolved in methanol (5.0 mL) was added dropwise to a methanol (8.0 mL) solution containing H_2heap (72.5 mg, 0.25 mmol) and piperidine (42.6 mg, 0.5 mmol). The mixture was refluxed with stirring for 5 h. The resulting blue solution was filtered and then equal volume of benzene was added. Blue crystals suitable for X-ray analysis were obtained from the solution by slow evaporation at room temperature for 1 week. Yield: 70.1 mg (52%). Anal. Calcd for $Cu_2C_{12}H_{24}N_6O_{10}$ (%): C, 26.7; H, 4.5; N, 15.6. Found (%): C, 26.6; H, 4.4; N, 15.7.

2.3. *Physical measurements*

The C, H, and N microanalyses were performed on a Perkin–Elmer 240 elemental analyzer. Molar conductance was measured with a Shanghai DDS-11A conductometer. Infrared spectrum was recorded on a Nicolet-470 spectrophotometer from 4000 to 400 cm^{-1} as KBr pellets. Electronic spectra were measured on a Cary 300 spectrophotometer; fluorescence spectra were measured with an Fp-750w Fluorometer. Cyclic voltammetric experiments were carried out using a CHI 832B electrochemical analyzer in connection with a glassy carbon working electrode (GCE), saturated calomel reference (SCE), and a platinum wire auxiliary electrode. The GCE surface was freshly polished to a mirror prior to each experiment with 0.05 μm α-Al_2O_3 paste and then cleaned in water.

2.4. *Crystal structure determination*

Diffraction data were collected on a Bruker APEX area-detector diffractometer using graphite-monochromated Mo-Kα radiation ($\lambda = 0.71073$ Å). The crystal structure was solved by the heavy atom method followed by Fourier syntheses. Structure refinement was performed by full-matrix least-squares procedures using SHELXL97 on F^2 [16]. Two uncoordinated oxygens of nitrate were disordered with free refined site occupancy factors of 0.52839 (O4A and O5A) and 0.47161 (O4B and O5B). The H atom of the hydroxyl was located in a difference Fourier map, all other hydrogens were placed in calculated positions with C–H = 0.97 Å and N–H = 0.91 Å, and included in the final cycles of refinement as riding mode, with $U_{iso}(H) = 1.2U_{eq}$ of the carrier atoms. Crystal data and refinement conditions are summarized in table 1.

2.5. *Antibacterial assays*

The bacteria used were *Staphylococcus aureus*, *Bacillus subtilis*, *Escherichia coli*, *Proteus vulgaris*, and *Pseudomonas aeruginosa*. The antibacterial activities of the ligand and the complex were determined qualitatively using the paper disc method with 100 mg mL^{-1} solutions in DMSO. A lawn of micro-organisms was prepared by pipetting and evenly spreading 100 µL of inoculum [adjusted turbidmetrically to 10^5–10^6 CFU mL^{-1} (CFU = colony forming units)] onto the nutrient agar set in Petri dishes. Paper discs of 6 mm diameter were impregnated with the stock solutions of these two compounds and dried under sterile conditions. Then the dried discs were laid on the previously inoculated agar surface. The plates were incubated at 37 ± 2°C. After 24 h the inhibition diameters were measured. The experiments were repeated three times and the results are expressed in average values.

Table 1. Crystal data and details of the structure determination of **1**.

Empirical formula	$C_{12}H_{24}Cu_2N_6O_{10}$
Formula weight	539.47
Crystal system	Monoclinic
Space group	*P2(1)/c*
Unit cell dimensions (Å, °)	
a	9.533(4)
b	7.202(3)
c	15.436(7)
α	90.00
β	106.152(6)
γ	90.00
Volume (Å^3), *Z*	1018.0(8), 2
Calculated density (g cm^{-3})	1.760
Absorption coefficient (mm^{-1})	2.152
Scan-mode	φ and ω scan
F(000)	552
Crystal size (mm^3)	0.26 × 0.22 × 0.19
θ range for data collection (°)	2.22–25.02
Limiting indices	$-11 < h < 10$; $-8 < k < 8$; $-18 < l < 17$
Total unique data, *R*(int)	4940, 1796, 0.0619
Observed data [$I > 2\sigma(I)$]	1029
R, wR_2	0.0498, 0.1130
S	0.957
Max., average shift/error	0.000, 0.000

In order to understand quantitatively the magnitude of the antibacterial activities, the antibacterial activities of the ligand, and the complex were evaluated for their minimum inhibitory concentration (MIC) values by the microdilution broth method. Compound solutions (100 mg mL^{-1}) were added to broth for different concentrations (range from 50 to 1000 μg mL^{-1}). Suspensions of the bacterial strains, with an optical density of McFarland 0.5 (10^7–10^8 CFU), were made in isotonic sodium chloride solution. Samples of each bacterial suspension were added to the serial dilution of the test substances. The inoculated test tubes were incubated at 37 ± 2°C under aerobic conditions. After 72 h the turbidity was evaluated. The MIC is defined as the lowest antimicrobial concentration of the test compounds which completely inhibit the bacterial growth. The experiments were repeated three times and the results are expressed in average values.

2.6. *DNA-binding studies*

All the experiments involving *HS*-DNA were performed in Tris-HCl buffer (pH = 7.92). Solution of DNA in Tris-HCl buffer solution gave a ratio of UV absorbances at 260 and 280 nm, A_{260}/A_{280}, of *ca* 1.9, indicating that the DNA was sufficiently free of protein [17]. The concentration of the prepared *HS*-DNA stock solution was determined from absorbance at 260 nm using $\varepsilon_{260} = 6600\ M^{-1}\ cm^{-1}$ [18]. Stock solution of the DNA was stored at 4°C and used after no more than 4 days. Electronic absorption titration and voltammetric studies were performed by keeping the concentration of the complex constant, while varying the *HS*-DNA concentration. In the ethidium bromide (EB) fluorescence displacement experiment, 5 μL of the EB Tris-HCl solution (1.0 mM L^{-1}) was added to 1 mL of DNA solution (at saturated binding levels [19]) and stored in the dark for 2 h. Then the solution of the dicopper(II) complex was titrated into the DNA/EB mixture and diluted in Tris-HCl buffer to 5 mL, producing solutions with varied mole ratio of the copper(II) complex to *HS*-DNA. Before measurements, the mixture was shaken and incubated at room temperature for 30 min. The fluorescence spectra of EB bound to DNA were obtained at an emission wavelength of 584 nm in the Fluorometer. Viscosity measurements were carried out using an Ubbelodhe viscometer immersed in a water bath maintained at 16(±0.l)°C. *HS*-DNA samples of approximately 200 base pairs in length were prepared by sonication in order to minimize the complexities arising from DNA flexibility [20]. Flow times were measured with a digital stopwatch, and each sample was measured three times, and an average flow time was calculated. Relative viscosities for *HS*-DNA in the presence and absence of the complex were calculated from the relation $\eta = (t - t_0)/t_0$, where t is the observed flow time of DNA-containing solution and t_0 is that of Tris-HCl buffer alone. Data were presented as $(\eta/\eta_0)^{1/3}$ *versus* [complex]/[DNA] [21], where η is the viscosity of DNA in the presence of the copper(II) complex and η_0 is that of DNA alone.

3. Results and discussion

3.1. *Synthesis of the dicopper(II) complex*

Two synthetic strategies are generally available for the preparation of binuclear complexes. One is to use a binucleating ligand which offers both the coordination

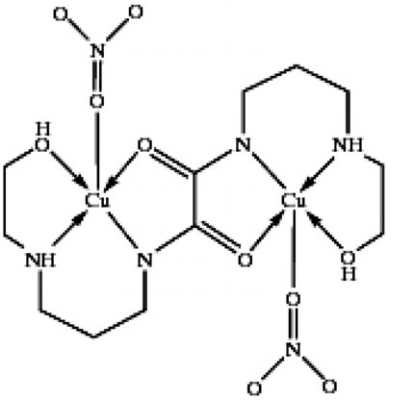

Scheme 1. The structure of $Cu_2(heap)(NO_3)_2$.

geometry and the ligand field strength suitable for metal ions. Another one is to use a "complex ligand" that contains a potential donor group capable of coordinating to another metal ion [6, 22–24]. In this study, our purpose was to obtain a Cu(II)–Cu(II) binuclear complex and the former synthetic method was adopted. As the binucleating ligand, we chose N,N′-bis(N-hydroxyethylaminopropyl)oxamide (H_2heap) (scheme 1), which can coordinate to metal ions through carbonyl oxygens and nitrogens of oxamido and also oxygens of hydroxyl [6]. In preparing the complex, the use of piperidine deprotonates H_2heap for coordination through oxamido nitrogens. Elemental analyses, IR and electronic spectral studies, and single-crystal X-ray diffraction indicate that the reaction of H_2heap with $Cu(NO_3)_2 \cdot 3H_2O$ in 1 : 2 mole ratio yielded the binuclear complex $Cu_2(heap)(NO_3)_2$.

3.2. *General properties of the dicopper(II) complex*

Molar conductance ($\Lambda = 170\,\Omega^{-1}\,cm^2\,mol^{-1}$ in $1.0 \times 10^{-3}\,mol\,L^{-1}$ methanol solution) of the dicopper(II) complex falls in the range of 1 : 2 electrolytes [25], suggesting that nitrates are situated outside the metal coordination sphere in solution. In the solid state the dicopper(II) complex is sufficiently stable in air to allow physical measurements.

3.3. *IR spectrum*

In the IR spectrum of the complex, the N–H and O–H vibrations of the bridging ligand are at 3390–2935 cm^{-1} and the C=O vibration is at 1624 cm^{-1}. Split bands at 1384 and 1357 cm^{-1} indicate the presence of monodentate nitrate [26], which is consistent with the crystal structure.

3.4. *Electronic spectrum*

In order to obtain further structural information of the dicopper(II) complex, the electronic spectrum of the complex ($1.0 \times 10^{-3}\,mol\,L^{-1}$) from 300 to 800 nm was

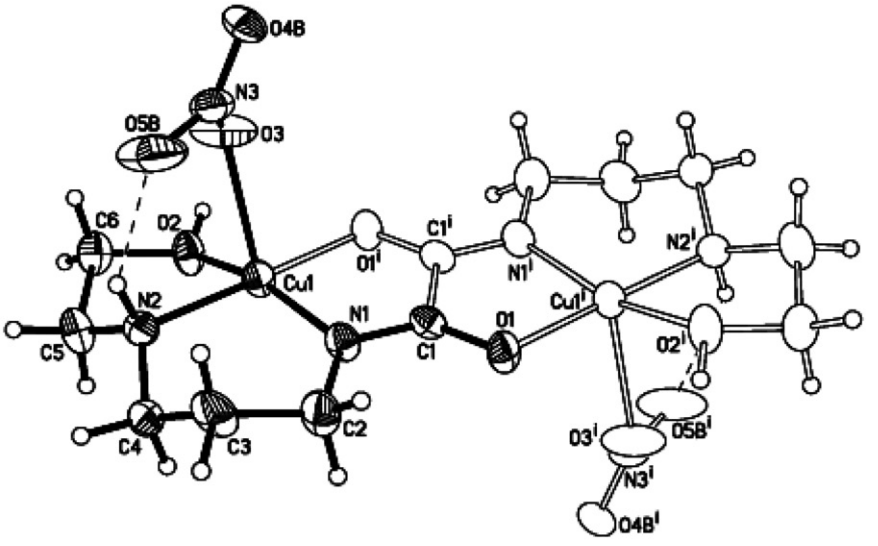

Figure 1. The molecular structure of **1** with atomic numbering scheme. Full displacement ellipsoids (for the asymmetric unit) and open ellipsoids (for the symmetry-related parts) are drawn at 30% probability. Only one disordered congener of nitrate is shown. Dashed lines indicate hydrogen bonds [symmetry code: (i) $2-x$, $1-y$, $1-z$].

measured in aqueous solution. A band centered at 616 nm ($\varepsilon = 95\,\mathrm{mol^{-1}\,dm^3\,cm^{-1}}$) can be unambiguously attributed to the d–d transition of copper(II). In addition, a strong absorption at 338 nm ($\varepsilon = 890\,\mathrm{mol^{-1}\,dm^3\,cm^{-1}}$) may be attributed to charge-transfer absorption, which may be due to spin-exchange interactions between copper(II) ions through the π-path orbital set up by an oxamido-bridge [6]. Further investigations of this and similar systems are required in order to obtain more detailed assignment for the charge transfer.

3.5. *Crystal structure*

The molecular structure of $Cu_2(heap)(NO_3)_2$ is illustrated in figure 1 and selected geometric parameters are summarized in table 2. The complex consists of a neutral centrosymmetric binuclear unit with an inversion center at the mid-point of the C1–C1^{i} bond [symmetry code: (i) $-x+2$, $-y+1$, $-z+1$]. The copper(II) has a square-pyramidal coordination geometry, with τ of 1.1, surrounded by N1, N2, O1^{i}, O2 from oxamido in the basal plane, and one oxygen (O3) from the nitrate in the apical position. The maximum displacement of the four atoms N1, N2, O1^{i}, O2 from the least-squares plane is 0.161(3) Å (O1^{i}) and copper(II) lies 0.162(3) Å out of this mean plane. The apical Cu–O distance of 2.341(6) Å is significantly longer than those in the basal plane (table 2), indicating weaker bonding between copper(II) and nitrate. The Cu1–N1 (amido) bond [1.932(5) Å] is shorter than the Cu1–N2 (sec-amino) bond [1.969(5) Å], consistent with stronger donor ability of the deprotonated amido nitrogen compared with the amino nitrogen [27, 28].

The bridging ligand is deprotonated at N1, and adopts a *bis*-tetradentate conformation, forming two five-membered and one six-membered chelate rings

Table 2. Selected bond distances (Å) and angles (°) for **1**.

Cu1–O1^{i}	1.951(4)	Cu1–O2	1.970(4)
Cu1–O3	2.341(6)	Cu1–N1	1.932(5)
Cu1–N2	1.969(5)	C1–O1	1.271(7)
C1–N1	1.280(8)	C1–C1^{i}	1.520(11)
O1^{i}–Cu1–O2	93.40(18)	O1^{i}–Cu1–O3	89.2(2)
O2–Cu1–O3	90.1(2)	N1–Cu1–O1^{i}	85.17(19)
N1–Cu1–O2	161.1(2)	N1–Cu1–O3	108.8(2)
N1–Cu1–N2	96.9(2)	N2–Cu1–O1^{i}	177.84(18)
N2–Cu1–O2	84.44(19)	N2–Cu1–O3	90.7(2)
N3–O3–Cu1	125.3(4)		

Symmetry code: (i) $2-x, 1-y, 1-z$.

Table 3. Distances (Å) and angles (°) of the hydrogen bonds for **1**.

D–H···A	*d*(D–H)	*d*(H···A)	*d*(D···A)	∠(D–H···A)
N2–H2C···O5A	0.91	2.52	3.21(2)	133.1
N2–H2C···O5B	0.91	2.27	3.07(4)	147.3
C3–H3A···O5A	0.97	2.50	3.34(2)	144.9
C4–H4A···O4A^{ii}	0.97	2.49	3.40(6)	156.3
C4–H4B···O5B^{v}	0.97	2.43	3.29(4)	147.4
C5–H5B···O1^{iii}	0.97	2.56	3.518(10)	168.5
O2–H2···O3^{iv}	0.93	2.32	3.050(7)	135.2
O2–H2···O4A^{iv}	0.93	1.76	2.67(4)	163.1
O2–H2···O4B^{iv}	0.93	1.93	2.83(5)	164.5

Symmetry codes: (ii) $x, 0.5-y, 0.5+z$; (iii) $x, y-1, z$; (iv) $2-x, y-0.5, 0.5-z$; (v) $1-x, y-0.5, 0.5-z$.

around each metal. The five-membered Cu1–O1^{i}–C1^{i}–C1–N1 ring is almost planar, whereas the other five-membered Cu1–O2–C6–C5–N2 ring has a twist conformation and the six-membered Cu1–N1–C2–C3–C4–N2 cycle adopts a half-chair conformation. The corresponding puckering parameters [29] are $\varphi = 262.5(7)^{\circ}$, $Q = 0.412(7)$ Å and $\varphi = 36.1(10)^{\circ}$, $Q = 0.503(8)$ Å, $\theta = 130.5(8)^{\circ}$. The oxamido-bridge is planar as observed in other oxamido-bridged copper(II) complexes [14, 15, 27, 30] and the Cu···Cu separation within the binuclear unit is 5.157(2) Å.

Hydrogen bonds lead to the formation of a 3-D supramolecular framework, which consists of two classical hydrogen bonds, N–H···O and O–H···O, and one non-classical hydrogen bond, C–H···O (table 3). As shown in figure 2, a 2-D infinite network paralleled to b0c plane is formed through hydrogen bonds between the hydroxyl and nitrate groups in different molecules. Adjacent layers are further connected by non-classical C4–H4B···O5B^{v} [symmetry code: (v) $1-x, y-0.5, 0.5-z$] to form a 3-D supramolecular architecture.

Comparing the crystal structure of **1** with that of the previously reported analogue $[Cu_2(heap)](ClO_4)_2 \cdot 2H_2O$ (**2**) [27], we find that the two complexes have essentially the same bridging ligand (heap) and metal ion (Cu^{2+}), thus, their IR and electronic spectra are similar. Both crystallize in *P2(1)/c*, however, their structures are different due to the replacement of perchlorate by nitrate. Copper(II) has a square pyramidal geometry in **1** instead of a square planar environment in **2** from increased coordination ability of nitrate; hence **1** is neutral while **2** contains a $[Cu_2(heap)]^{2+}$ cation in the solid.

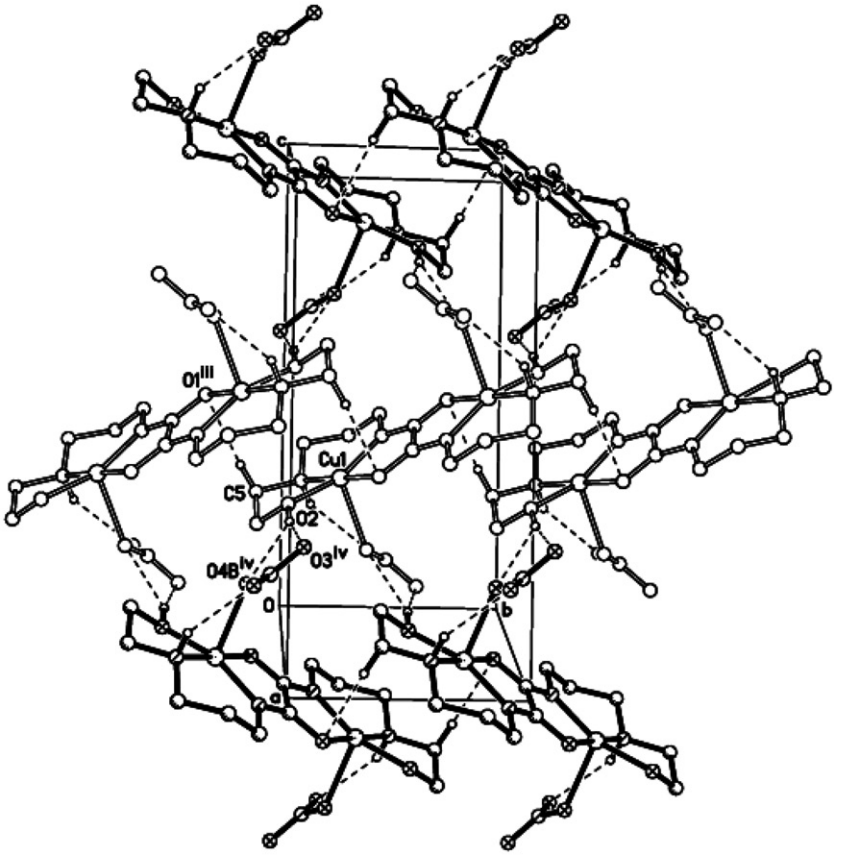

Figure 2. The 2-D hydrogen-bonded network paralleled to b0c plane. H atoms not involved in hydrogen bonds have been omitted for clarity [symmetry codes: (iii) x, $y-1$, z; (iv) $2-x$, $y-0.5$, $0.5-z$].

Though the complex molecules assemble to similar 2-D arrays *via* hydrogen bonds, in **1** the nitrate is the key in hydrogen bonding, while in **2** perchlorate needs lattice water molecule to complete the array. In addition, in **1** the C–H $\cdots$ O hydrogen bonds make the stack of 2-D arrays more stable than in **2**. The above discussion shows the importance of the counterion.

3.6. *Antibacterial activities*

Preliminary antibacterial screening and MIC values of the ligand and dicopper(II) complex are given in table 4. Both ligand and complex show activities against *S. aureus* and *E. coli* and inactivity against *B. subtilis*, *P. vulgaris*, and *Ps. aeruginosa*. The MIC values indicate that the complex shows better activity than the ligand against the same bacteria under identical experimental conditions due to the effect of the metal ion on cell process. Complexation considerably reduces the polarity of the metal ion because of the partial sharing of its positive charge with the donor groups. Such complexation could enhance the lipophilic character of the central metal atom, which subsequently favors permeation through the lipid layers of cell membrane [31]. On the other hand, by

Table 4. Qualitative and quantitative antibacterial assay [100 mg mL^{-1}; MIC value (μg mL^{-1})].

	Diameter of inhibition zone (mm)					MIC value (μg mL^{-1})	
Compound	*S. aureus*	*B. subtilis*	*E. coli*	*P. vulgaris*	*Ps. aeruginosa*	*S. aureus*	*E. coli*
Ligand	13	–	12	–	–	800	900
Complex	15	–	16	–	–	200	100

MIC: The minimum inhibitory concentration is the lowest concentration of a drug that inhibits more than 99% of the population.

comparing the results obtained in the antibacterial assay with those of the analogous complex (**2**) reported before [27], it can be concluded that the antibacterial results of the two complexes are close because they just have different counter anions.

3.7. *DNA binding studies*

3.7.1. Cyclic voltammetric studies. Cyclic voltammetry has been widely employed to study DNA-binding properties for complexes with electronic activity, whether the electrochemical processes are reversible [32], quasi-reversible [33], or irreversible [34, 35]. Before studying the interaction of $Cu_2(heap)(NO_3)_2$ with DNA, it is helpful to study the electrochemical behavior of the dicopper(II) complex in Tris-HCl buffer solution. The cyclic voltammograms of $Cu_2(heap)(NO_3)_2$ (5.0×10^{-4} m L^{-1}) at different scan rates (from 0.01 to 0.10 V s^{-1}) in the potential range between −0.9 and 0.2 V were investigated (Supplementary material). As the scan rates decreased from 0.10 to 0.01 V s^{-1}, the oxidation peak currents (I_{pa1}, I_{pa2}) and reduction peak currents (I_{pc1}, I_{pc2}, I_{pc3}) decrease and all are proportional to the square root of the scan rate ($\nu^{1/2}$). The results of linear correlation between I_{pa1}, I_{pa2}, I_{pc1}, I_{pc2}, I_{pc3} and $\nu^{1/2}$ are listed in table 5. These relationships indicate that the electrode processes in Tris-HCl buffer solution are diffusion controlled [36].

Restricting the scan rate to 0.10 V s^{-1}, the CV behaviors of $Cu_2(heap)(NO_3)_2$ (5.0×10^{-4} mol L^{-1}) without and with *HS*-DNA were studied and the results are given in figure 3. In the absence of DNA (curve **a**), the cyclic voltammogram displays two couples of redox peaks [couple 1: −0.164 V (E_{pc1}) and −0.006 V (E_{pa1}); couple 2: −0.421 V (E_{pc2}) and −0.118 V (E_{pa2})] which may correspond to Cu(II)Cu(II)/Cu(I)Cu(II) and Cu(I)Cu(II)/Cu(I)Cu(I), respectively, and one reduction peak at −0.598 V (E_{pc3}) corresponding to Cu(I)Cu(I)/Cu(I)Cu. The separations of anodic and cathodic peaks (ΔE_p) for couples 1 and 2 are 0.158 and 0.303 V with formal potentials of the free complex ($E_f^{\circ\prime}$) being −0.085 and −0.270 V. Upon the addition of *HS*-DNA (curve **b**), the peak currents decrease, and couple 2 and reduction peak 3 disappear; simultaneously, the formal potential of the bound complex ($E_b^{\circ\prime}$) of couple 1 [−0.164 V (E_{pc1}) and −0.070 V (E_{pa1})] shifts to more negative potential ($\Delta E^{\circ\prime} = E_b^{\circ\prime} - E_f^{\circ\prime} = -0.032$ V). These changes in the peak currents can be attributed to increased difficulty in the diffusion of the dicopper(II) complex bound to the large, slowly diffusing *HS*-DNA molecule [37]. Bard [38] has proposed that if $E^{\circ\prime}$ shifted to more negative value when small molecules interacted with DNA, the interaction

Table 5. Relationship between peak currents and the square root of the scan rate over a scan rate range from 0.01 to 0.10 V s^{-1}.

Plots of I *vs.* $v^{1/2}$	Linear equation	Correlation coeff. (r)
A	$y = 2 \times 10^{-4}x + 6 \times 10^{-6}$	0.9981
B	$y = 1 \times 10^{-4}x + 1 \times 10^{-6}$	0.9807
C	$y = 2 \times 10^{-5}x + 3 \times 10^{-6}$	0.9742
D	$y = 6 \times 10^{-5}x + 1 \times 10^{-6}$	0.9997
E	$y = 6 \times 10^{-5}x + 4 \times 10^{-6}$	0.9997

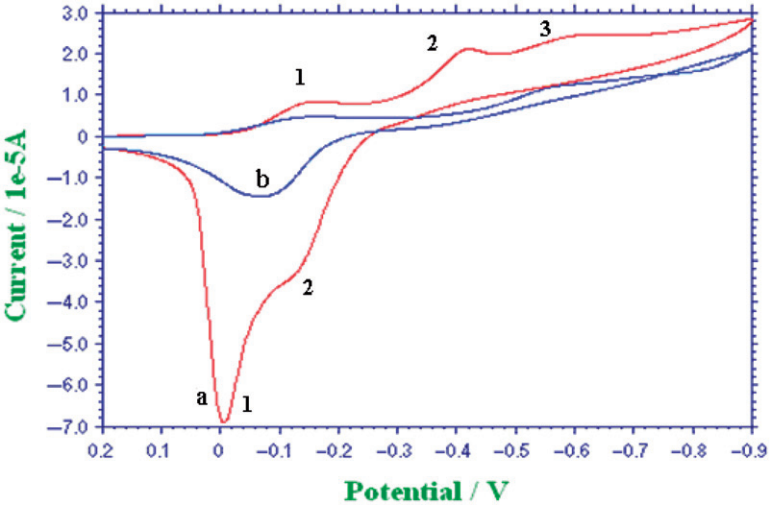

Figure 3. Cyclic voltammogram of **1** in the absence (a) and presence (b) of *HS*-DNA (1.5×10^{-3} mol L^{-1}) at 0.10 V s^{-1}.

mode was electrostatic. Otherwise, if $E^{\circ\prime}$ shifted to more positive value, the interaction mode was intercalative. Therefore, the shift to negative in $E^{\circ\prime}$ indicates that the interaction mode between the dinuclear copper(II) complex and *HS*-DNA is electrostatic. The shift in the value of the formal potential $\triangle E^{\circ\prime}$ can be used to estimate the ratio of equilibrium binding constants K_R/K_O according to the model of interaction described by Carter and Bard [39]. From this model one can obtain that:

$$\Delta E^{\circ\prime} = \Delta E_b^{\circ\prime} - \Delta E_f^{\circ\prime} = 0059 \log(K_R/K_O) \quad (1)$$

where K_R and K_O are the corresponding binding constants for the binding of reduced and oxidized species to DNA, respectively. For the dicopper(II) complex, the $K_{Cu(I)Cu(II)}/K_{Cu(II)Cu(II)}$ value was calculated to be 0.29, suggesting stronger binding affinity in the Cu(II)Cu(II) form compared to the Cu(I)Cu(II) form. Thus, according to electrochemical experiments, the binding mode of the dicopper(II) complex to *HS*-DNA is electrostatic, supported by the following electronic absorption titrations, EB fluorescence displacement experiments, and viscosity measurements.

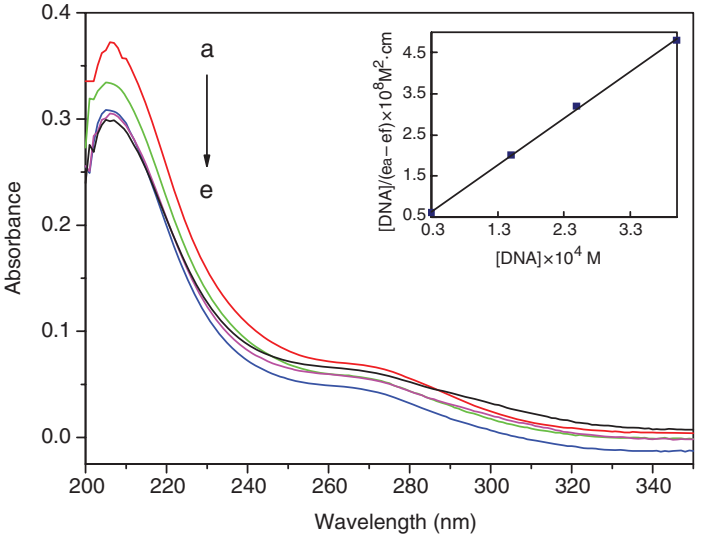

Figure 4. Electronic absorption spectra of the copper(II) complex upon the titration of *HS*-DNA. [complex] = 1.0×10^{-5} M L^{-1}; [DNA]: (a) 0, (b) 3.0×10^{-5}, (c) 1.5×10^{-4}, (d) 2.5×10^{-4} M L^{-1}, (e) 4.0×10^{-4} M L^{-1}. Arrow shows the absorbance upon the increasing *HS*-DNA concentrations. Inset: Plot of [DNA]/($\varepsilon_a - \varepsilon_f$) *vs.* [DNA] for the absorption titration of *HS*-DNA with the complex.

3.7.2. Electronic absorption titrations. To get a better insight into the interaction mode and binding strength between the dicopper(II) complex and *HS*-DNA, electronic absorption experiments were employed. Electronic absorption spectroscopy is an effective method to examine the binding modes and magnitudes of metal complexes with DNA. In general, hypochromism and red shift are associated with the binding of colored complexes to DNA, due to intercalative mode involving a strong stacking interaction between the aromatic chromophore of complexes and the base pairs of DNA [32, 40, 41]. The absorption spectra of the dicopper(II) complex (1.0×10^{-5} mol L^{-1}) in the absence and presence of *HS*-DNA ($3.0 \times 10^{-5} \sim 4.0 \times 10^{-4}$ mol L^{-1}) are given in figure 4. When titrated by *HS*-DNA, the dicopper(II) complex presents significant hypochromism centered at 206 nm absorption maximum, suggesting that the interaction between dicopper(II) complex and *HS*-DNA is different from classical intercalation [32, 40, 41]. These spectral features are similar to that which is interpreted as electrostatic interaction with DNA [42]. Cationic molecules can interact with DNA by neutralizing the negatively charged phosphate backbone of DNA [43]. Considering the weak coordination between the copper(II) and nitrate, the neutral dicopper(II) units in the solid state are cations and nitrate anions in solution (supported by molar conductivity). Therefore, it is likely that the positive dicopper(II) complex may facilitate the electrostatic interaction when interacting with *HS*-DNA in Tris-HCl buffer [42].

In order to understand quantitatively the magnitudes of the binding strength of the dicopper(II) complex, the intrinsic binding constant (K_b) is determined by using the following equation [44]:

$$[\mathrm{DNA}]/(\varepsilon_a - \varepsilon_f) = [\mathrm{DNA}]/(\varepsilon_b - \varepsilon_f) + 1/K_b(\varepsilon_b - \varepsilon_f) \quad (2)$$

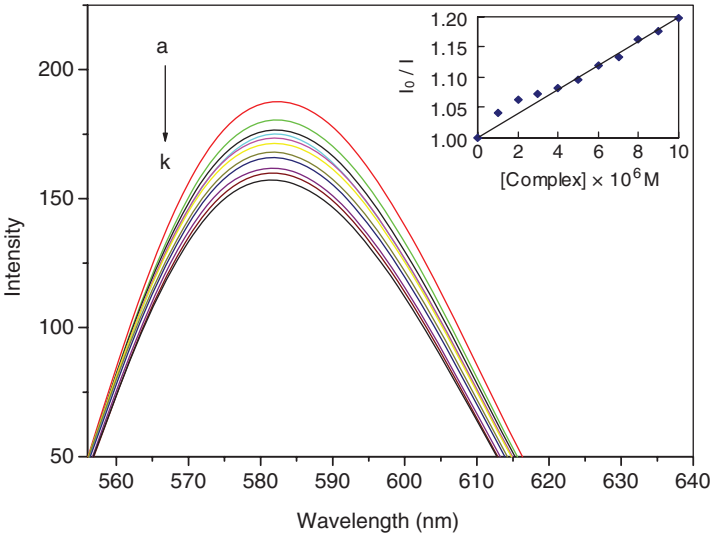

Figure 5. Emission spectra of the *HS*-DNA–EB system upon titration of the copper(II) complex. $\lambda_{ex} = 522$ nm; [EB] $= 1.0 \times 10^{-6}$ M L^{-1}; [DNA] $= 1.5 \times 10^{-3}$ M L^{-1}; [complex]: (a) 0, (b) 1.0×10^{-6}, (c) 2.0×10^{-6}, (d) 3.0×10^{-6}, (e) 4.0×10^{-6}, (f) 5.0×10^{-6}, (g) 6.0×10^{-6}, (h) 7.0×10^{-6}, (i) 8.0×10^{-6}, (j) 9.0×10^{-6}, (k) 1.0×10^{-5} ML^{-1}. Arrow shows the change upon increasing complex concentration. Inset: Plot of I_0/I *vs.* [complex] for titration of the copper(II) complex to *HS*-DNA–EB system.

where [DNA] is the concentration of *HS*-DNA, ε_f, ε_a and ε_b correspond to the extinction coefficient, respectively, for the free dicopper(II) complex, for each addition of DNA to the dicopper(II) complex and for the dicopper(II) complex in the fully bound form. The ratio of slope to intercept in the plot of [DNA]/($\varepsilon_a - \varepsilon_f$) *versus* [DNA] gives the value of K_b as 3.33×10^4 M^{-1} ($R = 0.9996$ for four points).

3.7.3. The EB fluorescence displacement experiments. Fluorescence titration experiments, especially the EB fluorescence displacement experiment, have been widely used to characterize the interaction of complexes with DNA by following changes in fluorescence intensity. The intrinsic fluorescence intensity of DNA is very low, and that of EB in Tris buffer is also not high due to quenching by the solvent molecules. However, on addition of DNA, the fluorescence intensity of EB is enhanced by intercalation into the DNA. Thus, EB can be used to probe the interaction of complexes with DNA. The fluorescence intensity of EB can be quenched by the addition of a molecule to the displacement of EB from DNA [45]. In our experiment (figure 5), the fluorescence intensity of EB bound to DNA at 584 nm shows remarkable decrease with increasing concentration of the dicopper(II) complex, suggesting that dicopper(II) complex binds strongly with DNA, consistent with our cyclic voltammetric studies and electronic absorption spectral results. The quenching of EB bound to DNA by the dicopper(II) complex is in agreement with the linear Stern–Volmer equation [46]:

$$I_0/I = 1 + K_{sv}[Q] \quad (3)$$

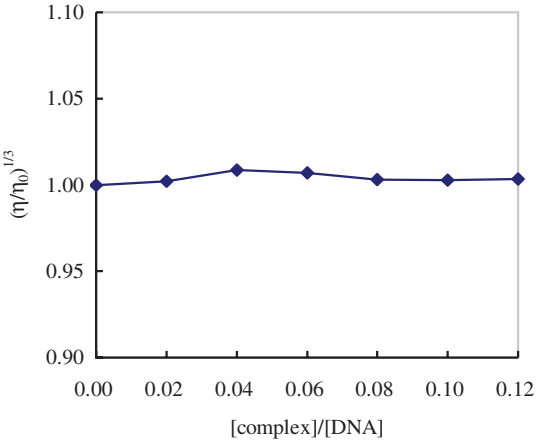

Figure 6. Effect of increasing amount of the complex on the relative viscosity of *HS*-DNA at 16(±0.1)°C, [DNA] = 0.2 mM.

where I_0 and I represent the fluorescence intensities in the absence and presence of quencher, respectively. K_{sv} is a linear Stern–Volmer quenching constant and Q is the concentration of quencher. In the quenching plot (inset in figure 5) of I_0/I *versus* [complex], K_{sv} is given by the ratio of the slope to intercept. The K_{sv} value for **1** is 2.01×10^5 ($R = 0.983$ for 11 points). Considering the strong interaction of EB with the DNA of which the binding constant of EB with DNA is $1.40 \times 10^6\,M^{-1}$ in Tris–HCl buffer [47], we thought it was impossible for the copper(II) complex to scramble EB from DNA. Similar fluorescence quenching effect of EB bound to DNA has been observed for the addition of several electrostatic binding compounds [48]. The present observation leads us to suspect that the copper(II) complex may interact with DNA through the electrostatic binding, releasing EB from EB-DNA system.

3.7.4. Viscosity measurements. To clarify further the interaction of the complex and *HS*-DNA, viscosity measurements were carried out. In intercalation, the DNA helix lengthens as base pairs are separated to accommodate the bound ligand leading to increased DNA viscosity; in electrostatic mode the length of the helix is unchanged resulting in no apparent alteration in DNA viscosity [49]. Viscosity is regarded as the least ambiguous means of studying the binding of metal complexes with DNA [50]. The effect of dicopper(II) complex on the viscosity of *HS*-DNA are shown in figure 6. As illustrated in this figure, on increasing the amount of **1**, the relative viscosity of *HS*-DNA remains essentially unchanged, very similar to that observed for other complexes which interacted with DNA in electrostatic mode [51]. Thus, the viscosity measurement is consistent with the results of the cyclic voltammetric studies, electronic absorption titrations, and EB fluorescence displacement experiments.

Considering the structure of the dicopper(II) complex and the DNA-binding results observed in the voltammetric studies, electronic absorption titrations, EB fluorescence displacement experiments, and viscometry measurements, one can conclude that the electrostatic binding is the most probable interaction mode between the binuclear copper(II) complex and *HS*-DNA. The static electrostatic interaction likely occurred

between the positive charge in the complex and the negative phosphate backbone of *HS*-DNA [33].

Indeed, further investigations are still required by using other methods in order to get a reasonable explanation and a deeper insight into the DNA-binding mode of the complexes with oxamido-bridge and are in progress in our laboratory.

Supplementary material

Crystallographic data (excluding structure factors) for the structure reported in this work have been deposited at the Cambridge Crystallographic Data Center and allocated the deposition number: CCDC 633222.

Acknowledgments

This project was supported by the National Natural Science Foundation of China (No. 30672515) and the PhD Programs Foundation of Ministry of Education of China (No. 20060423005).

References

[1] C.A. Reed, R.D. Orosz. In *Spin Coupling Concepts in Bioinorganic Chemistry*, C.J. O'Connor (Ed.), World Scientific, Singapore (1993).
[2] D. Gatteschi, O. Kahn, J.S. Miller, F. Palacio (Eds.), *Molecular Magnetic Materials*, NATO ASI Series, Kluwer, Dordrecht (1991).
[3] S. Thyagarajan, N.N. Murthy, A.A.N. Sarjeant, K.D. Karlin, S.E. Rokita. *J. Am. Chem. Soc.*, **128**, 7003 (2006).
[4] T. Biver, C. Cavazza, F. Secco, M. Venturini. *J. Inorg. Biochem.*, **101**, 461 (2007).
[5] Q.Q. Zhang, F. Zhang, W.G. Wang, X.L. Wang. *J. Inorg. Biochem.*, **100**, 1344 (2006).
[6] H. Ojima, K. Nonoyama. *Coord. Chem. Rev.*, **92**, 85 (1988).
[7] Z.N. Chen, H.X. Zhang, K.B. Yu, B.S. Kang, H. Cai, C.Y. Su, T.W. Wang, Z.L. Lu. *Inorg. Chem.*, **37**, 4775 (1998).
[8] R. Ruiz, J. Faus, F. Lloret, M. Julve, Y. Journaux. *Coord. Chem. Rev.*, **193–195**, 1069 (1999).
[9] Z.L. Liu, Z.L. Lu, D.Q. Zhang, Z.H. Jiang, L.C. Li, C.M. Liu, D.B. Zhu. *Inorg. Chem.*, **43**, 6620 (2004).
[10] S.W. Bi, C.B. Liu, H.Q. Hu. *J. Phys. Chem. B*, **106**, 10786 (2002).
[11] Y.T. Li, C.W. Yan, J. Zhang. *Cryst. Growth Des.*, **4**(3), 481 (2003).
[12] Y.T. Li, C.W. Yan, S.H. Miao, D.Z. Liao. *Polyhedron*, **17**(15), 2491 (1998).
[13] Y.T. Li, C.W. Yan, H.S. Guan. *Synth. Met.*, **144**, 69 (2004).
[14] Y.T. Li, C.Y. Zhu, G.Q. Li, C.W. Yan, G.Y. Xu. *Transition Met. Chem.*, **30**, 850 (2005).
[15] Y.T. Li, C.W. Yan, Z.Y. Wu, C.Y. Zhu. *J. Magn. Magn. Mater.*, **292**, 418 (2005).
[16] G.M. Sheldrick. *SHELXL97, Program for Crystal Structure Refinement*, University of Göttingen, Germany (1997).
[17] J. Marmur. *J. Mol. Biol.*, **3**, 208 (1961).
[18] M.E. Reichmann, S.A. Rice, C.A. Thomas, P.J. Doty. *J. Am. Chem. Soc.*, **76**, 3047 (1954).
[19] J.K. Barton, J.M. Goldberg, C.V. Kumar, N.J. Turro. *J. Am. Chem. Soc.*, **108**, 2081 (1986).
[20] J.B. Chaires, N. Dattagupta, D.M. Crothers. *Biochemistry*, **21**, 3933 (1982).
[21] G. Cohen, H. Eisenberg. *Biopolymers*, **8**, 45 (1969).
[22] K. Nakatani, J. Sletten, S. Hault-Desporte, S. Jeannin, Y. Jeannin, O. Kahn. *Inorg. Chem.*, **30**, 164 (1991).

[23] P. Yu, O. Kahn, K. Nakatani, E. Codjovi, C. Mathoniere, J. Sletten. *J. Am. Chem. Soc.*, **113**, 6558 (1991).
[24] O. Kahn. *Struct. Bonding (Berlin)*, **68**, 89 (1987).
[25] W.J. Geary. *Coord. Chem. Rev.*, **7**, 81 (1971).
[26] H. Okawa, N. Matsumoto, M. Koikawa, K. Takeda, S. Kida. *J. Chem. Soc., Dalton Trans.*, 1383 (1990).
[27] C.Y. Zhu, Y.T. Li, Z.Y. Wu, Y.L. Song. *J. Coord. Chem.*, **60**(4), 465 (2007).
[28] J.K. Tang, Y. Ou Yang, H.B. Zhou, Y.Z. Li, D.Z. Liao, Z.H. Jiang, S.P. Yan, P. Cheng. *Cryst. Growth Des.*, **5**(2), 813 (2005).
[29] D. Cremer, J.A. Pople. *J. Am. Chem. Soc.*, **97**, 1354 (1975).
[30] F. Lloret, M. Julve, J. Faus, Y. Journaux, M. Philoche-Levisalles, Y. Jeannin. *Inorg. Chem.*, **28**, 3702 (1989).
[31] B.G. Tweedy. *Phytopathologh*, **55**, 910 (1964).
[32] S. Mahadevan, M. Palaniandavar. *Inorg. Chem.*, **37**, 693 (1998).
[33] Y. Li, Y. Wu, J. Zhao, P. Yang. *J. Inorg. Biochem.*, **101**, 283 (2007).
[34] X. Hu, K. Jiao, W. Sun, J.Y. You. *Electroanalysis*, **6**, 613 (2006).
[35] Y. Zhang, Y. Cai, S. Su, Y. Ni. *Electroanalysis*, **15**, 1479 (2006).
[36] A.J. Bard, L.R. Faulkner. *Electrochemical Methods*, John Wiley & Sons Inc., New York (1980).
[37] M. Rodriguez, A.J. Bard. *Anal. Chem.*, **62**, 2658 (1990).
[38] M.T. Carter, M. Rodriguez, A.J. Bard. *J. Am. Chem. Soc.*, **111**, 8901 (1989).
[39] M.T. Carter, A.J. Bard. *J. Am. Chem. Soc.*, **109**, 7528 (1987).
[40] V.A. Bloomfield, D.M. Crothers, I. Tinoc. *Physical Chemistry of Nucleic Acids*, Harper and Row, New York (1974).
[41] J. Liu, H. Zhang, C. Chen, H. Deng, T. Lu, L. Ji. *J. Chem. Soc., Dalton Trans.*, 114 (2003).
[42] Y.N. Xiao, C.X. Zhan. *J. Appl. Polym. Sci.*, **84**, 887 (2002).
[43] L. Strekowski, B. Wilson. *Mutat. Res.*, **623**, 3 (2007).
[44] A.M. Pyle, J.P. Rehmann, R. Meshoyrer, C.V. Kumar, N.J. Turro, J.K. Barton. *J. Am. Chem. Soc.*, **111**, 3051 (1989).
[45] R. Indumathy, S. Radhika, M. Kanthimathi, T. Weyhermuller, B.U. Nair. *J. Inorg. Biochem.*, **101**, 434 (2007).
[46] J.R. Lakowiez, G. Webber. *Biochemistry*, **12**, 4161 (1973).
[47] J.B. Le Pecq, C. Paoletti. *J. Mol. Biol.*, **27**, 87 (1967).
[48] R. Senthil Kumar, S. Arunachalam. *Polyhedron*, **25**, 3113 (2006).
[49] S. Satyanarayana, J.C. Dabrowiak, J.B. Chaires. *Biochemistry*, **32**, 2573 (1993).
[50] S. Satyanarayana, J.C. Dabrowiak, J.B. Chaires. *Biochemistry*, **31**, 9319 (1992).
[51] C.W. Jiang, H. Chao, H. Li, L.N. Ji. *J. Inorg. Biochem.*, **93**, 247 (2003).